App. Envi. Res. 44(3) (2022): 88-100

Applied Environmental Research

Journal homepage : http://www.tci-thaijo.org/index.php/aer

Magnetization of a Biochar Derived from Orange Peel and Its Application for the Removal of Crystal Violet

Issam Boudraa[1,5,*], Sevde Ustun Odabasi[2], Maryam Bareera[3], Hassan Ayadi[1,4], Brahim Kebabi[5], Hanife Buyukgungor[2]

[1] Department of chemistry, 20 Août 1955 University, Algeria
[2] Department of Environmental Engineering, Ondokuz Mayis University, Samsun Turkey
[3] Department of environmental science, University of Gujrat, Pakistan
[4] Research Unit of Environmental Chemistry, and Structural Molecular, Constantine1 University, Algeria
[5] Laboratoire de pollution et traitement des eaux, université Constantine1, Alegria

[*] Corresponding author: issam.boudraa@umc.edu.dz

Article History
Submitted: 25 May 2022/ Revision received: 12 September 2022/ Accepted: 14 September 2022/ Published online: 29 September 2022

Abstract

In this work, biochar synthesized from orange peel modified with magnetite was used as an alternative magnetic adsorbent for dye removal. The magnetization of the synthesized biochar was done using the co-precipitation method. The obtained composite was characterized by X-ray diffraction (XRD), Scanning electron microscopy (SEM), and Raman spectroscopy. The efficiency of magnetized biochar (OPB/Fe_3O_4) was studied in the process of removing crystal violet (CV) from an aqueous solution at different temperatures. The experimental data obtained for the kinetic studies were better fitted to the pseudo-second-order model, and the isotherms data were well fitted to the Langmuir model. The results showed that the adsorption capacity increases with increasing temperature, reaching 113 mg g^{-1} at 50 °C. Thermodynamic parameters (ΔG^0, ΔH^0, ΔS^0) were also calculated; their values showed that the adsorption was spontaneous and endothermic. These results inspire us to use other similar materials to solve the problem of water and environmental pollution.

Keywords: Adsorption; Co-precipitation; Magnetite; Dye removal; Raman spectroscopy; X-ray diffraction

Introduction

The pollution of water resources with industrial effluents containing organic compounds and toxic substances is a great concern. Generally, waste effluents from textile industries, paper printing, and photography contain residues of dyes and chemicals. Crystal violet (CV) is one of the synthetic dyes widely used in the textile industry and it's frequently present in industrial wastewater through industrial discharges. CV is potentially dangerous for human health [1] and can persist in the environment for a long time, posing serious problems [2].

https://doi.org/10.35762/AER.2022.44.3.7

Several techniques exist for the removal of pollutants from wastewater, such as catalytic oxidation [3], membrane separation [4], electrocoagulation [5], and adsorption [6]. The adsorption process is widely used to remove various types of pollutants from wastewater due to its simplicity, high efficiency, facility of use, and other advantages. The synthesis of suitable adsorbents with low cost has been the subject of researchers worldwide in the last few years [7–9]. Many studies have been performed to valorize biomass with biochar production for its use as an adsorbent for different pollutants [10–17]. Generally, biochars are considered among the suitable adsorbents for different types of pollutants. However, separating and reusing the biochar powders from the aqueous solutions is difficult after the adsorption process. Magnetization of biochar has been proposed by different researchers to solve this problem [18–22]; this modification allows the separation of biochar easily using a permanent magnet. The modification of the adsorbents with nanoparticles of magnetite (Fe_3O_4) is the most frequent and the most important due to their low cost, ease of synthesis, and good chemical and magnetic properties of the magnetite [23–26].

Magnetic solid phase extractions have recently been investigated as a new environmental treatment process [27]. However, only a few iron nanoparticles modified adsorbent were tested [28–30]. Using biochar, combining sustainable magnetic and modified adsorbent for green chemistry has been less explored. When the literature studies are examined, it is seen that there is no dye removal study with magnetic biochar produced from orange peel and this study is unique in this respect. Therefore, in this study aimed to develop magnetic biochar derived from orange peel using an easy and low cost co-precipitation method to remove organic pollutants. The obtained composite was tested for CV removal by evaluating adsorption kinetics, isotherm study, and thermodynamics parameters. This study also contributes to enriching knowledge on the valorization of biomasses as precursors for manufacturing of magnetic adsorbents for pollutant removal.

Materials and methods

Ferric chloride hexahydrate ($FeCl_3 \cdot 6H_2O$), ferrous sulfate heptahydrate ($FeSO_4 \cdot 7H_2O$), ammonium hydroxide (NH_4OH, 25% of ammonia), Crystal violet (C.I. 42555) were purchased from Merck.

1) Preparation of biochar (OPB)

Orange peel (Citrus sinensis) was collected in winter from the Black sea region in Turkey. The raw materials were washed and oven-dried at 80 °C for 48 h and then cut into small pieces in the range of 3–4 mm. The obtained biomass was crushed, milled, and rinsed with tap water followed by slightly acidic water (pH 5.5), prepared with 0.1M H_2SO_4 in the ratio of 1:10, to remove any charged species from the peel surface. After acid washing, biomass was washed with distilled water and dried at 80 °C overnight. The fraction of particle diameter between 250 to 500 µm was selected to prepare the biochar. 20 g from the selected powdered biomass was pyrolyzed for one hour in the presence of a steady flow of nitrogen (150 $cm^3\ min^{-1}$) at 400°C.

2) Preparation of modified biochar (OPB/Fe_3O_4)

The magnetic biochar (OPB/Fe_3O_4) was prepared with a 3:1 weight ratio. 1.5 g from the obtained biochar and 1.17 g of $FeCl_3 \cdot 6H_2O$ had been suspended in a 500 mL round bottom flask with distilled water under stirring for 12 h. After that, 0.6 g $FeSO_4 \cdot 7H_2O$ was added to the mixture and heated under a nitrogen (N_2) atmosphere until 85 °C, noting that the quantities of iron salts have been calculated considering the stoichiometric coefficients of the formation of magnetite Eq. (1).

$$2\ FeCl_3 + FeSO_4 + 8\ NH_4OH = Fe_3O_4 + (NH_4)_2SO_4 + 6\ NH_4Cl + 4\ H_2O \quad \text{(Eq. 1)}$$

At this stage, aqueous ammonia (25 %) was added to the mixture to ensure the formation of magnetite. The obtained solid was separated by centrifugation, washed several times with distilled water, and dried in an oven at 80 ºC for 12 h. The magnetization of the obtained composite was tested with a simple magnet.

3) Characterization

OPB and OPB/Fe_3O_4 were characterized using several techniques XRD, SEM, and Raman spectroscopy. XRD was collected using a Rigaku smart Lab X-Ray diffractometer, with Cu-Kβ radiation in the range of 2θ = 10–80° with steps of 0.01°. Scanning electron microscopy images were taken with JEOL (JSM-7001F), and the accelerating voltage was 5 kV. Raman spectra were recorded on a Horiba Lab RAM HR Evolution Micro-Raman spectrometer in the wave number range of 1000–2000 cm^{-1}.

4) The point of zero charge

The point of zero charge (pzc) of OPB/ Fe_3O_4 was also determined. Six beakers containing 50 mg of OPB/Fe_3O_4 and 50 mL of NaCl (0.1 M) were adjusted at different pHi = 2, 4, 6, 8, 10, 12 using HCl (0.1M) and NaOH (0.1M). After a contact time of 48 h under shaking, the final pH (pHf) was measured. The pzc was determined from the curve (pHf - pHi) as a function of pHi.

5) Kinetic study

In different flasks, 50 mg of the adsorbent was mixed with 50 mL of CV dye solutions at a concentration of 150 mg L^{-1}. Each sample was shaken with a constant speed of 100 rpm in a shaker at room temperature and free pH (pH = 6.5). After magnetic separation using a simple magnet (Figure 1), final concentrations were measured using UV/VIS spectrophotometry at different times (2, 4, 8, 12, 20, 25, 30, 60, 120, and 240 min). (Thermo, Uv-Vis Genesys 10S) at λ_{max} = 590 nm. The quantity of the absorbed CV at time t was calculated using the following Eq. 2.

$$q_t = \frac{V(C_o - C_t)}{m} \quad \text{(Eq. 2)}$$

Where q_t (mg g^{-1}) is the quantity of absorbed dye at time t (min), C_o (mg L^{-1}) and C_t (mg L^{-1}) are the initial concentration, the concentration at time t, respectively, and V (L) is the volume of the solution, and m (g) is the weight of adsorbent.

The removal efficiency of the adsorbent was calculated as follows:

$$R\ (\%) = \frac{C_i - C_e}{C_i} \times 100 \quad \text{(Eq. 3)}$$

Where C_i is the initial CV concentration (mg L^{-1}), C_e is the equilibrium concentration of MB solution (mg L^{-1}).

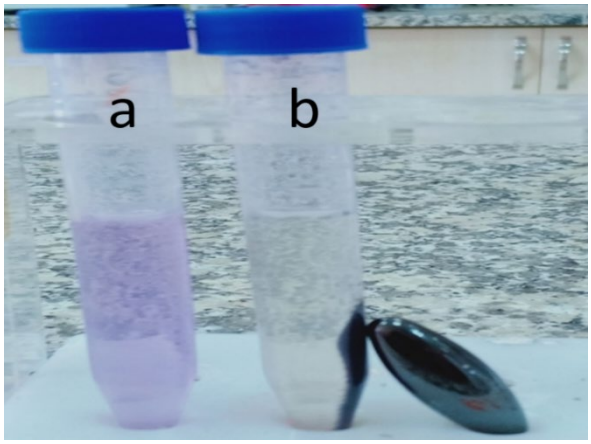

Figure 1 Test separation with a simple magnet, a) CV before adsorption, b) CV after adsorption, and magnetic separation.

6) Adsorption equilibrium

The adsorption equilibrium isotherms were realized at three temperatures, 30, 40, and 50 °C. In eight flasks, 50 mg of adsorbent was mixed

with different CV solutions with concentrations from 20 to 250 mg L^{-1} and at free pH (pH = 6.5). All flasks were shaken at 100 rpm for 4 h. Final concentrations of CV in eight flasks after 4 h were measured at λ_{max} = 590 nm using UV/VIS spectrophotometry. The amount of CV adsorbed was determined using the following Eq. 4.

$$q_e = \frac{V(C_0 - C_e)}{m} \quad \text{(Eq. 4)}$$

Where q_e (mg g^{-1}) is the quantity of the absorbed dye in the solid phase, C_e (mg L^{-1}) is the concentration of CV at equilibrium, C_o (mg L^{-1}) is the initial concentration, and V (L) is the volume of the solution.

Results and discussion

1) Characterization of OPB and OPB/Fe_3O_4

XRD patterns of OPB and OPB/Fe_3O_4 are shown in Figure 2. An Extended signal between intervals of 2θ between 18°–25° was observed in the diffractograms of OPB, indicating the presence of amorphous carbon [31–32], the presence of a peak at 2θ = 43.25° confirm also the presence of certain degree of graphitic carbon [33–34]. In addition, the XRD patterns displayed other peaks at 2θ = 25°, 32°, 39°, and 48° which can be attributed to the presence of hydroxyapatite in the biochar (ICDD-PDF No 00-001-1008) [24]. On the other hand, the appearance of some peaks at 2θ = 30°, 35°, 37° can be attributed to the presence of SiO_2 and alkali salts such as $CaCO_3$ [35–36]. The diffraction lines in the second patterns of OPB/Fe_3O_4 were observed at 2θ = 30.09°, 35.64°, 42.82, 57.97°and 62.94° corresponding to (220), (311), (400), (511) and (440) reflections, respectively (ICDD-PDF No. 00-025-1376) confirmed the presence of magnetite in the mixture [37].

SEM analysis was performed to examine the morphological structure of OPB and OPB/Fe_3O_4. Figure 3 shows a clear difference in the biochar surface before and after magnetization. It was noticed that the surface morphology of the OPB grains was irregular in the first image (Figure 3a and 3b), and post-modification (Figure 3c and 3d), it was observed also that the surface of the biochar was modified and contained small particles of magnetite.

Figure 4 indicates Raman spectra of biochar and magnetized biochar samples. The first peak, around 1364 cm^{-1} designated to the D band of stretching vibrations of non-graphitic carbons. The second peak observed at 1582 cm^{-1} represents the G band of stretching vibrations of graphitic carbons. The value of ID/IG represents the amount of non-graphitic carbons relative to graphitic carbons in the biochar and magnetized biochar. Generally, the increase of defects in graphical carbon increase the capacity of storage and adsorption [38]. In our composite, the value of ID/IG increased from 0.77 for biochar to 1.01 for magnetized biochar; those values confirm that the modification of the biochar magnetite created more defects and decreased the percentage of graphical carbons, which is a good parameter for the increase of the adsorption capacity [39–42].

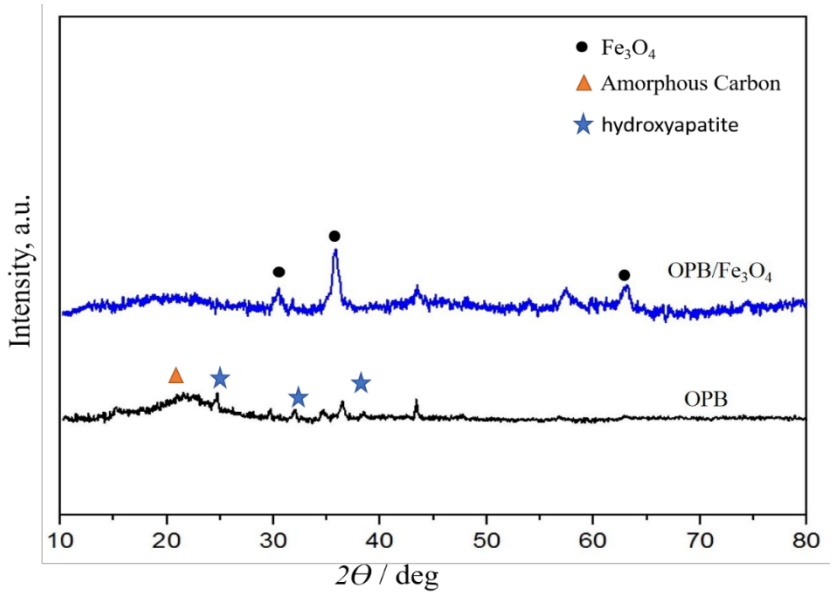

Figure 2 XRD spectra of OPB and OPB/Fe_3O_4.

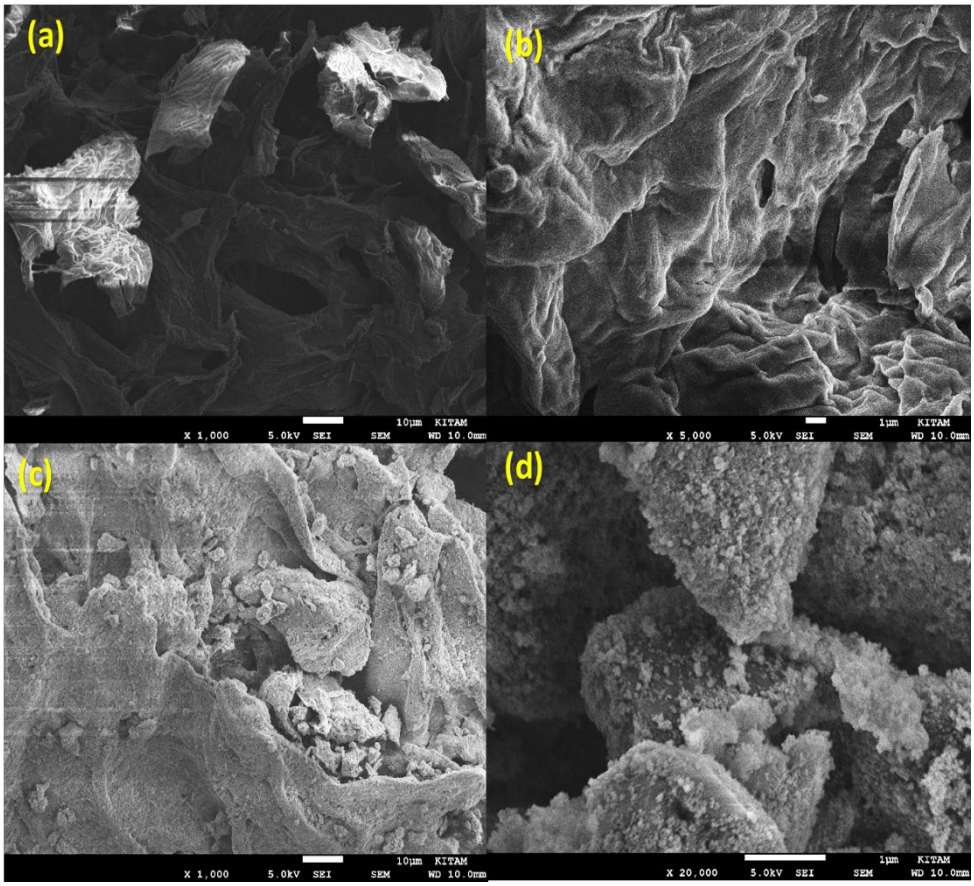

Figure 3 SEM images of (a), (b) OPB x1000 and x5000 magnifications and (c), (d) OPB/Fe_3O_4 with x1000 and x20000 magnifications.

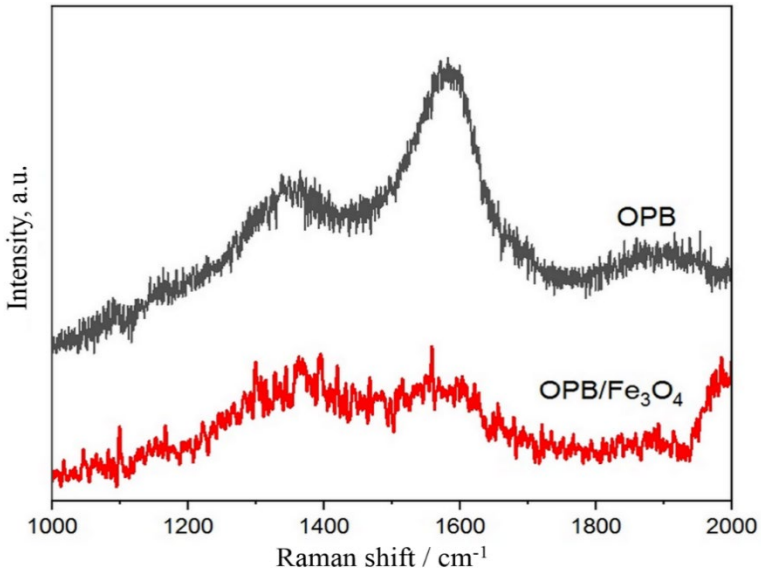

Figure 4 Raman spectra of OPB and OPB/Fe_3O_4.

2) Kinetic studies

For kinetic studies, the two most used models, the pseudo-first-order Eq. 5 and pseudo-second order [43] Eq. 6 are applied to understand the adsorption process of CV on OPB/Fe_3O_4 [44].

$$q_t = q_e\left(1 - \exp^{-k_1 t}\right) \quad \text{(Eq. 5)}$$

$$q_t = \frac{q_e^2 k_2 t}{1 + k_2 q_e t} \quad \text{(Eq. 6)}$$

While k_1 (min^{-1}) and k_2 (g mg^{-1} min^{-1}) represent the kinetic constants of pseudo-first-order and pseudo-second-order models, respectively; q_e (mg g^{-1}) and q_t (mg g^{-1}) represent the amount adsorbed per gram of adsorbent at equilibrium and at time t (min) respectively. The normalized standard evaluated the fit to the models. The application of the pseudo-first-order and pseudo-second-order on the experimental data (Figure 5) indicates that the pseudo-second-order adsorption kinetic model best describes the adsorption of CV on the surface of the OPB/Fe_3O_4 with height values of the correlation coefficient (R^2 = 0.99). This explains that the amount of CV adsorbed on the OPB/Fe_3O_4 is insignificant at low concentrations. As this concentration increases, the amount absorbed increases to reach a saturation level at high concentrations.

The calculated parameters k_1, k_2, q_e, and R^2 are summarized in Table 1. The necessary time to reach the equilibrium was around 150 min. CV is a cationic dye, and the surface charge of OPB/Fe_3O_4 is negative at pH > pHpzc. Knowing that the value obtained from the point of zero charge was pHpzc = 3.86 and the solution pH = 6.5, these parameters contributed to creating electrostatic interactions and played a role in eliminating CV.

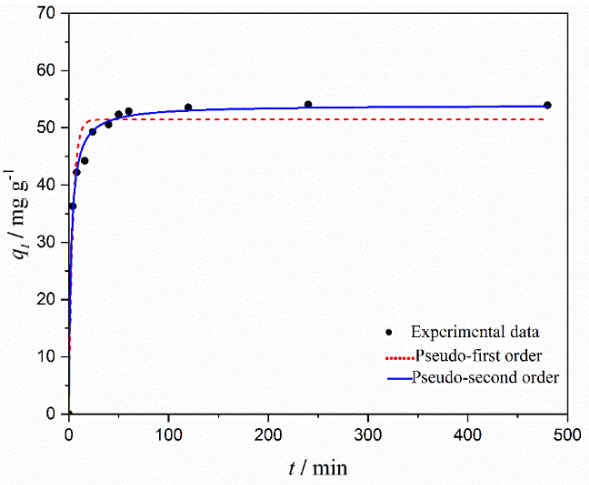

Figure 5 Adsorption kinetics of CV on OPB/Fe_3O_4 and the fit of experimental data with the pseudo-first-order and pseudo-second-order models.

Table 1 Kinetics parameters of CV dye adsorption on OPB/Fe_3O_4 were obtained from the adjustment of non-linearized pseudo-first-order and pseudo-second-order models

Adsorbent	q_{exp} (mg g^{-1})	Pseudo-first order	Pseudo-second order
OPB/Fe_3O_4	54.06	$q_{e,cal}$ = 51.44	$q_{e,cal}$ = 53.97
		k_1 = 0.258	$k_2 = 8 \cdot 10^{-4}$
		R^2 = 0.967	R^2 = 0.994

3) Adsorption equilibrium

The obtained results of the adsorption equilibrium of CV dye on OPB/Fe_3O_4 were fitted using the two most used models: Langmuir [45] Eq. 7 and Freundlich [46] Eq. 8.

$$q_e = \frac{q_m K_L C_e}{1+K_L C_e} \quad \text{(Eq. 7)}$$

Where q_e is equilibrium adsorption (mg g^{-1}), q_m (mg g^{-1}) is the maximum adsorption capacity, C_e (mg L^{-1}) is the liquid phase concentration of dye at the time (t), and k_L (L mg^{-1}) is the Langmuir constant.

$$q_e = K_F C_e^{1/n} \quad \text{(Eq. 8)}$$

Where K_F is the Freundlich coefficient, q_e (mg g^{-1}) is the amount of the adsorbed dye at equilibrium, and C_e (mg L^{-1}) is the liquid phase concentration of dye at the time (t).

The obtained values of the removal efficiency of the adsorbent are 86.9, 90.18, and 96.21 % for 30 °C, 40 °C and 50 °C, respectively.

Figure 6 presents the relevant results of the experimental data with Langmuir and Freundlich isotherms models at 30 °C, 40 °C, and 50 °C of the adsorption of CV dye on OPB/Fe_3O_4. The obtained values of R^2 from the isotherm study showed that the experimental data of the three isotherms at 30 °C, 40 °C, and 50 °C were fitting best using the Langmuir model compared to the Freundlich model with values of R^2 up to 94 % (Table 2). The maximum adsorption value was obtained at 50 °C. The Langmuir isotherm describes in a simple way the formation of a monolayer of adsorbate on the surface of the adsorbent.

4) Determination of the specific area

In our study, Langmuir isotherm is the adequate description of the adsorption of CV onto OPB/Fe_3O_4. The knowledge of q_m leads to the determination of the surface S_L using the following Eq. 9 [46–49].

$$S_L = (q_m \times a_{CV} \times N_A \times 10^{-23})/M \quad \text{(Eq. 9)}$$

Where, S_L (m^2 g^{-1}) is the specific surface area; qm (mg g^{-1}) is the maximum adsorption capacity obtained from the Langmuir model, a_{CV} is the occupied surface area of one molecule of Crystal violet = 585.9Å2 [50], and M (g mol^{-1}) is the molar mass of crystal violet = 407.98 g mol^{-1}. The obtained values (Table 2) correlate well with the literature [51].

Compared to some previous studies (Table 3), the obtained values of the removal of CV with OPB/Fe_3O_4 (113 mg g^{-1}) look promising and indicate that the OPB/Fe_3O_4 is an efficient adsorbent for organic pollutants removal.

5) Thermodynamic parameters

To evaluate the thermodynamic nature of CV adsorption process by OPB/Fe_3O_4, the thermodynamic parameters, namely Gibbs free change (ΔG^0), enthalpy change (ΔH^0), and entropy change (ΔS^0), were calculated using the following equations [57–58].

$$\ln k_c = -\frac{\Delta H^0}{RT} + \frac{\Delta S^0}{R} \quad \text{(Eq. 10)}$$

$$\Delta G^0_{ads} = -RT\ln k_c \quad \text{(Eq. 11)}$$

$$k_c = \frac{C_e \text{ (adsorbent)}}{C_e \text{ (solution)}} \quad \text{(Eq. 12)}$$

Where k_c is the equilibrium constant of adsorption, Ce (adsorbent) is the concentration of the adsorbed CV on the adsorbent at equilibrium, and Ce (solution) is the concentration of the CV solution at equilibrium.

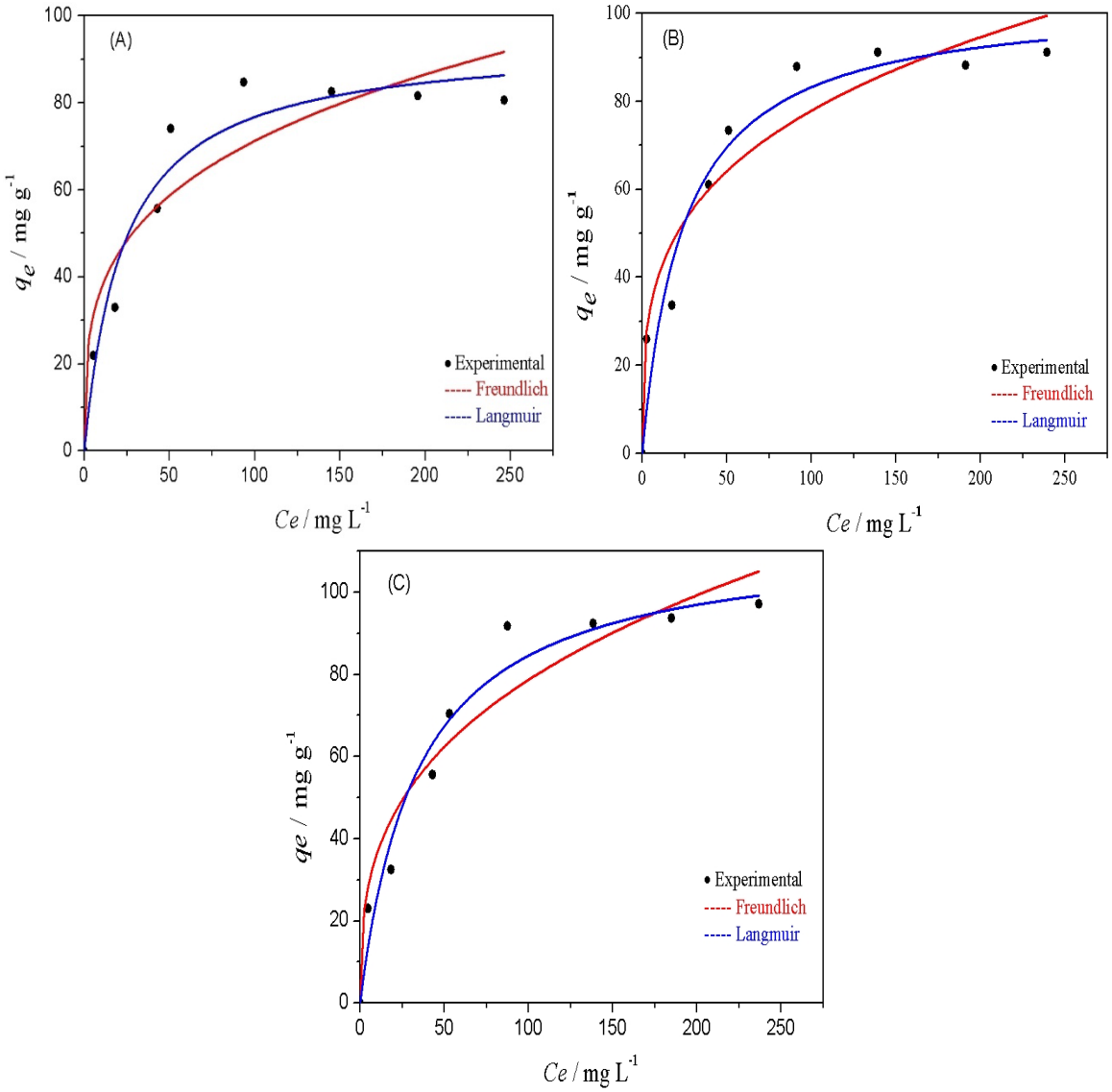

Figure 6 The fitting of experimental data of the adsorption of CV on OPB/Fe_3O_4 with Langmuir and Freundlich models at temperatures of (A) 30 °C, (B) 40 °C, and (C) 50 °C.

Table 2 Parameters of the different models for the adsorption of CV on OPB/Fe_3O_4

Parameters		Temperature		
		30 °C	**40 °C**	**50 °C**
Langmuir	k_L (L mg^{-1})	0.044	0.040	0.030
	q_m (mg g^{-1})	94.33	103.56	113.62
	R^2	0.9570	0.9462	0.9543
	S_L (m^2 g^{-1})	815.91	895.75	982.77
Freundlich	k_F (L mg^{-1})	19.63	21.44	16.80
	1/n	0.28	0.28	0.33
	R^2	0.8823	0.9304	0.9134

Table 3 Adsorption capacities of reported adsorbents for crystal violet

Adsorbent	pH	Q_e (mg g^{-1})	Reference
Charred rice husks	10	62.85	[52]
Xanthated rice husks	10	90.02	[52]
Gum acacia cross-linked poly(acryl amide)	9	90.90	[53]
Jute fiber carbon	8	27.99	[54]
Magnetic nanocomposite	8.5	113.13	[55]
CarAlg/MMt Nanocomposite hydrogels	6.4	88.80	[56]
Magnetized biochar	6.5	113.62	This sudy

Table 4 Thermodynamic parameters obtained for the adsorption of CV on OPB/Fe_3O_4

Temperature	ΔG^0 (kJ mol^{-1})	ΔH^0 (kJ mol^{-1})	ΔS^0 (J mol^{-1} K^{-1})
30 °C	-0.519	3.738	14.05
40 °C	-0.659		
50 °C	-0.800		

The values of ΔH^0 and ΔS^0 were determined from the slope ($-\Delta H^0/R$) and intercept ($\Delta S^0/R$) of the plot of ln k_d versus 1/T (Figure 7), respectively.

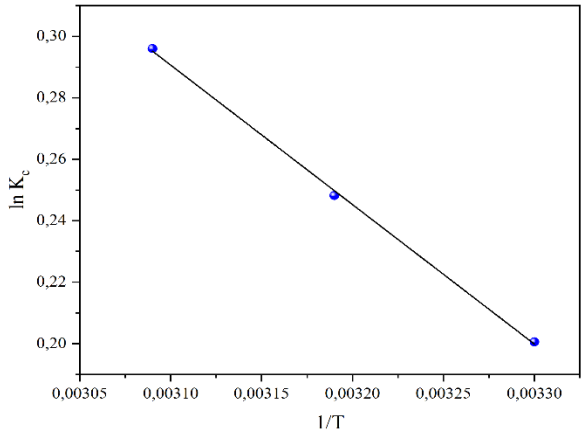

Figure 7 Plot of (ln kc) versus 1/T.

The calculated thermodynamic parameters at three temperatures (30, 40, and 50 °C) are shown in Table 4. The positive value of ΔH^0 indicates that the adsorption process of CV on OPB/Fe_3O_4 is endothermic in nature. While the negative values of ΔG^0 show the spontaneous nature of the adsorption. The positive value of ΔS^0 suggests an increase in the randomness at the solid/solution interface during the adsorption process [59].

Conclusion

In this study a synthetized biochar from orange peel was successfully magnetized using coprecipitation method. The magnetic biochar exhibited a good effectively of Crystal violet removal. The results of adsorption kinetics and isotherms analysis showed that crystal violet adsorptions by the magnetized biochar were better fitted using pseudo-second-order model and Langmuir model respectively. The removal efficiency reaches 96.21% at 50 °C with adsorption capacity of 113 mg g^{-1}. The values of the calculated thermodynamic parameters suggest that the adsorption process is spontaneous and endothermic. The magnetization of the biochar increases defects and oxygen bonds at the surface, which increase the capacity of adsorption. This indicate that it is easy and feasible to prepare a magnetized adsorbent from orange peel as a potential sorbent for environmental applications.

References

[1] Fabryanty, R., Valencia, C., Soetaredjo, F.E., Putro, J.N., Santoso, S.P., Kurniawan, A., Ju, Y.H., Ismadji, S. Removal of crystal violet dye by adsorption using bentonite-alginate composite. Journal of Environ-

mental Chemical Engineering, 2017, 5(6), 5677–5687.

[2] Mani, S., Bharagava, R.N. In Reviews of Environmental contamination and toxicology Volume 237; de Voogt, W. P., Ed.; Springer International Publishing: Cham, 2016, 237, 71–104.

[3] Ruan, Y., Kong, L., Zhong, Y., Diao, Z., Shih, K., Hou, L.A., Wang, S., Chen, D. Review on the synthesis and activity of iron-based catalyst in catalytic oxidation of refractory organic pollutants in wastewater. Journal of Cleaner Production, 2021, 321, 128924.

[4] Wang, Y., Zhang, W., Zeng, X., Deng, T., Wang, J. Membranes for separation of alkali/alkaline earth metal ions: A review. Separation and Purification Technology, 2021, 278, 119640.

[5] Titchou, F.E., Zazou, H., Afanga, H., El Gaayda, J., Akbour, R. A., Hamdani, M. Removal of persistent organic pollutants (POPs) from water and wastewater by adsorption and electrocoagulation process. Groundwater for Sustainable Development, 2021, 13, 100575.

[6] Şentürk, İ., Alzein, M. Adsorptive removal of basic blue 41 using pistachio shell adsorbent - Performance in batch and column system. Sustainable Chemistry and Pharmacy, 2020, 16, 100254.

[7] Ivanovska, A., Pavun, L., Dojcinovic, B., Kostic, M. Kinetic and isotherm studies for nickel ions' biosorption by jute fabrics. Journal of the Serbian Chemical Society, 2021, 86(9), 885–897.

[8] Şentürk, İ., Alzein, M. Adsorption of acid violet 17 onto acid-activated pistachio shell: Isotherm, kinetic and thermodynamic studies. Acta Chimica Slovenica, 2020, 67(1), 55–69.

[9] Mathurasa, L., Damrongsiri, S. Potential of using surfactants to enhance ammonium and nitrate adsorption on rice husk and its biochar. Applied Environmental Research, 2017, 39(1), 11–22.

[10] Geçgel, Ü., Kocabıyık, B., Üner, O. Adsorptive removal of methylene blue from aqueous solution by the activated carbon obtained from the fruit of catalpa bignonioides. Water, Air, & Soil Pollution, 2015, 226(8), 238.

[11] Luana A.R. Giusto, F.L.P., Talita S. Castro & fabiano magalhães preparation of activated carbon from sugarcane bagasse soot and methylene blue adsorption. Water, Air, & Soil Pollution, 2017, 228 (7), 249.

[12] Chen, J., Ouyang, J., Lai, W., Xing, X., Zhou, L., Liu, Z., Chen, W., Cai, D. Synthesis of ultralight chitosan/activated biochar composite aerogel globules for ketoprofen removal from aqueous solution. Separation and Purification Technology, 2021, 279, 119700.

[13] Haris, M., Hamid, Y., Usman, M., Wang, L., Saleem, A., Su, F., ..., Li, Y. Crop-residues derived biochar: Synthesis, properties, characterization and application for the removal of trace elements in soils. Journal of Hazardous Materials, 2021, 416, 126212.

[14] Kumar, S.A., Aier, I., Pathak, S., Anand, A., Jha, S., Vijay, V.K., Kaushal, P. Copper (II) removal from aqua solution using rice straw derived biochar. Materials Today: Proceedings, 2021, 43, 740–745.

[15] Şentürk, İ., Yıldız, MR. Highly efficient removal from aqueous solution by adsorption of Maxilon Red GRL dye using activated pine sawdust. Korean Journal of Chemical Engineering, 2020, 37(6), 985–999.

[16] Zhang, X., Zhang, S., Yang, H., Shao, J., Chen, Y., Liao, X., ..., Chen, H. Generalized two-dimensional correlation infrared spectroscopy to reveal mechanisms of CO_2 capture in nitrogen enriched

biochar. Proceedings of the Combustion Institute, 2017, 36(3), 3933–3940.

[17] Bella, H., Bendaikha, H. Biochar from empty date fruit bunch as an Adsorbent to rmove eriochrome black T and methylene blue from aqueous solution. Applied Environmental Research, 2022, 44–55.

[18] Han, Z., Sani, B., Mrozik, W., Obst, M., Beckingham, B., Karapanagioti, H.K., Werner, D. Magnetite impregnation effects on the sorbent properties of activated carbons and biochars. Water Research, 2015, 70, 394–403.

[19] Oladipo, A.A., Ifebajo, A.O. Highly efficient magnetic chicken bone biochar for removal of tetracycline and fluorescent dye from wastewater: Two-stage adsorber analysis. Journal of Environmental Management, 2018, 209, 9–16.

[20] Imran, M., Khan, Z.U.H., Iqbal, M.M., Iqbal, J., Shah, N.S., Munawar, S., ..., Rizwan, M. Effect of biochar modified with magnetite nanoparticles and HNO_3 for efficient removal of Cr(VI) from contaminated water: A batch and column scale study. Environmental Pollution, 2020, 261, 114231.

[21] Bai, S., Zhu, S., Jin, C., Sun, Z., Wang, L., Wen, Q., Ma, F. Sorption mechanisms of antibiotic sulfamethazine (SMT) on magnetite-coated biochar: pH-dependence and redox transformation. Chemosphere, 2021, 268, 128805.

[22] Wang, F., Li, L., Iqbal, J., Yang, Z., Du, Y. Preparation of magnetic chitosan corn straw biochar and its application in adsorption of amaranth dye in aqueous solution. International Journal of Biological Macromolecules, 2022, 199, 234–242.

[23] Ranjithkumar, V., Hazeen, A.N., Thamilselvan, M., Vairam, S. Magnetic activated carbon-Fe_3O_4 nanocomposites-synthesis and applications in the removal of acid yellow dye 17 from water. Journal of Nanoscience and Nanotechnology, 2014, 14(7), 4949–4959.

[24] de Melo, N.H.n., de Oliveira Ferreira, M. E.n., Silva Neto, E.M., Martins, P.R., Ostroski, I.C.ú. Evaluation of the adsorption process using activated bone char functionalized with magnetite nano-particles. Environmental Nanotechnology, Monitoring & Management, 2018, 10, 427–434.

[25] Mu, Y., Du, H., He, W., Ma, H. Functionalized mesoporous magnetic biochar for methylene blue removal: Performance assessment and mechanism exploration. Diamond and Related Materials, 2022, 121, 108795.

[26] Zhang, H., Li, R., Zhang, Z. A versatile EDTA and chitosan bi-functionalized magnetic bamboo biochar for simultaneous removal of methyl orange and heavy metals from complex wastewater. Environmental Pollution, 2022, 293, 118517.

[27] Du, C., Song, Y., Shi, S., Jiang, B., Yang, J., Xiao, S. Preparation and characterization of a novel Fe_3O_4-graphene-biochar composite for crystal violet adsorption. Science of the Total Environment, 2020, 711, 134662.

[28] Ghaedi, M., Hajjati, S., Mahmudi, Z., Tyagi, I., Agarwal, S., Maity, A., Gupta, V.K. Modeling of competitive ultrasonic assisted removal of the dyes – Methylene blue and Safranin-O using Fe_3O_4 nanoparticles. Chemical Engineering Journal, 2015, 268, 28–37.

[29] Nasiri, S., Alizadeh, N. Synthesis and adsorption behavior of hydroxypropyl-beta-cyclodextrin-polyurethane magnetic nanoconjugates for crystal and methyl violet dyes removal from aqueous solutions. RSC Advances, 2019, 9(42), 24603–24616.

[30] Sun, P., Hui, C., Azim Khan, R., Du, J., Zhang, Q., Zhao, Y.H. Efficient removal of crystal violet using Fe_3O_4-coated biochar: The role of the Fe_3O_4 nanoparticles

and modeling study their adsorption behavior. Scientific Reports, 2015, 5, 12638.

[31] Morales, L.F., Herrera, K., Lopez, J.E., Saldarriaga, J.F. Use of biochar from rice husk pyrolysis: assessment of reactivity in lime pastes. Heliyon, 2021, 7(11), e08423.

[32] Pusceddu, E. Comparison between ancient and fresh biochar samples, a study on the recalcitrance of carbonaceous structures during soil incubation. International Journal of New Technology and Research, 2017, 3, 39–46.

[33] Gonzalez-Canche, N.G., Carrillo, J.G., Escobar-Morales, B., Salgado-Transito, I., Pacheco, N., Pech-Cohuo, S.C., Pena-Cruz, M.I. Physicochemical and optical characterization of citrus aurantium derived biochar for solar absorber applications. Materials (Basel), 2021, 14(16).

[34] Xu, Y., Zhang, X., Wu, B., Xu, Y., Wen, R., Liu, Y., ..., Huang, Z. Preparation and performance of shape-stable phase change materials based on carbonized-abandoned orange peel and paraffin. Fullerenes, Nanotubes and Carbon Nanostructures, 2019, 27(4), 289–298.

[35] Zhang, D., Wang, T., Zhi, J., Zheng, Q., Chen, Q., Zhang, C., Li, Y. Utilization of jujube biomass to prepare biochar by pyrolysis and activation: Characterization, adsorption characteristics, and mechanisms for nitrogen. Materials (Basel), 2020, 13 (24).

[36] Dehkhoda, A.M., Ellis, N., Gyenge, E. Electrosorption on activated biochar: Effect of thermo-chemical activation treatment on the electric double layer capacitance. Journal of Applied Electrochemistry, 2013, 44(1), 141–157.

[37] Salimi, P., Norouzi, O., Pourhoseini, S.E. M., Bartocci, P., Tavasoli, A., Di Maria, F., ..., Fantozzi, F. Magnetic biochar obtained through catalytic pyrolysis of macroalgae: A promising anode material for Li-ion batteries. Renewable Energy, 2019, 140, 704–714.

[38] Olsson, E., Cottom, J., Cai, Q. Defects in hard carbon: Where are they located and how does the location affect alkaline metal storage? Small, 2021, 17(18), e2007652.

[39] Chen, X., Lin, Q., He, R., Zhao, X., Li, G. Hydrochar production from watermelon peel by hydrothermal carbonization. Bioresource Technology, 2017, 241, 236–243.

[40] Xiao, X., Chen, B. A direct observation of the fine aromatic clusters and molecular structures of biochars. Environmental Science & Technology, 2017, 51(10), 5473–5482.

[41] Subratti, A., Vidal, J.L., Lalgee, L.J., Kerton, F.M., Jalsa, N.K. Preparation and characterization of biochar derived from the fruit seed of Cedrela odorata L and evaluation of its adsorption capacity with methylene blue. Sustainable Chemistry and Pharmacy, 2021, 21, 100421.

[42] Abbaci, F., Nait-Merzoug, A., Guellati, O., Harat, A., El Haskouri, J., Delhalle, J., ..., Guerioune, M. Bio/KOH ratio effect on activated biochar and their dye based wastewater depollution. Journal of Analytical and Applied Pyrolysis, 2022, 162, 105452.

[43] de Melo, N.H., de Oliveira Ferreira, M.E., Silva Neto, E.M., Martins, P.R., Ostroski, I.C. Evaluation of the ad-sorption process using activated bone char functionalized with magnetite nanoparticles. Environmental Nanotechnology, Monitoring & Management, 2018, 10, 427–434.

[44] Ho, Y.S., McKay, G. Pseudo-second order model for sorption processes. Process Biochemistry, 1999, 34(5), 451–465.

[45] Sahmoune, M.N. Evaluation of thermodynamic parameters for adsorption of heavy metals by green adsorbents. Environmental Chemistry Letters, 2018, 17(2), 697–704.

[46] Pasukphun, N., Suma, Y. Preliminary study of color removal from Moh Hom

dyeing wastewater using a low cost activated carbon derived from pineapple waste. Applied Environmental Research, 2017, 39(3), 41–47.

[47] Avom, J., Mbadcam, J.K., Matip, M.R. L., Germain, P. Adsorption isotherme de l'acide acétique par des charbons d'origine végétale. African Journal of Science and Technology, 2009, 2(2).

[48] Kaewprasit, C., Hequet, E., Abidi, N., Gourlot, J.P. Application of methylene blue adsorption to cotton fiber specific surface area measurement: Part I. metho-dology. The Journal of Cotton Science, 1998, 2.

[49] Itodo, A.U., Itodo, H.U., Gafar, M.K. Estimation of specific surface area using Langmuir isotherm method. Journal of Applied Sciences and Environmental Management, 2011, 14(4).

[50] Güzel, F., Sayğılı, H., Sayğılı, G.A., Koyuncu, F. Decolorisation of aqueous crystal violet solution by a new nanoporous carbon: Equilibrium and kinetic approach. Journal of Industrial and Engineering Chemistry, 2014, 20(5), 3375–3386.

[51] Ai, T., Jiang, X., Zhong, Z., Li, D., Dai, S. Methanol-modified ultra-fine magnetic orange peel powder biochar as an effective adsorbent for removal of ibuprofen and sulfamethoxazole from water. Adsorption Science & Technology, 2020, 38(7–8), 304–321.

[52] Homagai, P.L., Poudel, R., Poudel, S., Bhattarai, A. Adsorption and removal of crystal violet dye from aqueous solution by modified rice husk. Heliyon, 2022, 8(4), e09261.

[53] Sharma, G., Kumar, A., Naushad, M., Garcia-Penas, A., Al-Muhtaseb, A.H., Ghfar, A.A., ..., Stadler, F.J. Fabrication and characterization of Gum arabic-cl-poly(acrylamide) nanohydrogel for effective adsorption of crystal violet dye. Carbohydrate Polymers, 2018, 202, 444–453.

[54] Porkodi, K., Vasanth, K.K. Equilibrium, kinetics and mechanism modeling and simulation of basic and acid dyes sorption onto jute fiber carbon: Eosin yellow, malachite green and crystal violet single component systems. Journal of Hazardous Materials, 2007, 143(1–2), 311–327.

[55] Singh, K.P., Gupta, S., Singh, A.K., Sinha, S. Optimizing adsorption of crystal violet dye from water by magnetic nanocomposite using response surface modeling approach. Journal of Hazardous Materials, 2011, 186(2–3), 1462–1473.

[56] Mahdavinia, G.R., Aghaie, H., Sheykhloie, H., Vardini, M.T., Etemadi, H. Synthesis of CarAlg/MMt nanocomposite hydrogels and adsorption of cationic crystal violet. Carbohydrate Polymers, 2013, 98(1), 358 –365.

[57] Liu, Y. Is the free energy change of adsorption correctly calculated?. Journal of Chemical & Engineering Data, 2009, 54(7), 1981–1985.

[58] Bonilla-Petriciolet, A.n., Mendoza-Castillo, D.I., Reynel-Ávila, H.E. Adsorption processes for water treatment and purification. Springer International Publishing: Cham, 2017, 1–18.

[59] Rani, S., Sud, D. Effect of temperature on adsorption-desorption behaviour of triazophos in Indian soils. Plant, Soil and Environment, 2015, 61(1), 36–42.